Properties of alkali activated slag-fly ash blends with limestone addition

Cement & Concrete Composites 59 (2015) 119–128

Contents lists available at ScienceDirect

Cement & Concrete Composites

journal homepage: www.elsevier.com/locate/cemconcomp

Properties of alkali activated slag–fly ash blends with limestone addition

X. Gao *, Q.L. Yu, H.J.H. Brouwers

Department of the Built Environment, Eindhoven University of Technology, P.O. Box 513, 5600 MB Eindhoven, The Netherlands

ARTICLE INFO

Article history:
Received 12 December 2014
Received in revised form 28 January 2015
Accepted 29 January 2015
Available online 21 March 2015

Keywords:
Alkali activation
Slag–fly ash blends
Limestone
Reaction kinetics
Fresh behavior
Mechanical property

ABSTRACT

In this article, the effects of raw materials' composition on fresh behavior, reaction kinetics, mechanical properties and microstructure of alkali activated slag–fly ash–limestone blends are investigated. The results indicate that, with the increasing content of fly ash and limestone, the slump flow increases. The setting times are shortened when increasing the slag content, while both fly ash and limestone show a negligible influence. The reaction process is slightly accelerated by the presence of limestone due to the extra provided nucleation sites, but the reaction process is mainly governed by the slag. The slag content exhibits a dominant role on strength in this ternary system, while for a constant slag content, the compressive strength increases with the increasing limestone content up to 30%. The microstructure analysis shows that the gel characteristics are independent of the limestone powder content. The presence of limestone in initially high Ca and Al conditions does not lead to the formation of additional crystalline phases, which is different from Portland cement systems. Both physically and chemically bound water contents are slightly increased when limestone powder is incorporated.

1. Introduction

The utilization of alkali activated materials (AAMs) as a substitute for ordinary Portland cement has attracted great attention in recent years. This type of material generally exhibits better performance, such as enhanced mechanical properties [1], durability [2,3], thermal properties [4] and lower environmental impacts [5] when compared to ordinary Portland cement. Alkali activated materials can be classified into two types according to the calcium content in the raw materials [6]. One is the high calcium system, the typical precursor is ground granulated blast furnace slag (GGBS), having a C–A–S–H type gel as the main reaction product [7]. Class F fly ash and metakaolin are representative raw materials for the low calcium system, having N–A–S–H type gels within a three-dimensional network as the major reaction product [8]. However, although excellent performances can be achieved from both systems, drawbacks that limit their practical application are also obvious such as fast setting, high shrinkage of alkali activated slag [9,10] and the requirement of elevated curing temperatures, as well as the relatively long setting times of alkali activated aluminosilicates [11,12].

Approaches to avoid the disadvantages in individual system were widely studied; among those studies, attention was paid to blended alkaline systems (Na_2O–CaO–Al_2O_3–SiO_2 systems) that are produced by mixing calcium enriched precursors and aluminosilicates, due to the modified properties such as setting times [13], workability [14], shrinkage [15], mechanical properties and durability [16]. The reaction products in the blended system are C–A–S–H, N–A–S–H and calcium substituted (N,C)–A–S–H type gels [17,18] with a higher degree of cross-linking [19] that are simultaneously formed during the activation, indicating an ideal gel compatibility. Besides, the influences of key manufacturing factors on reaction kinetics, gel characteristics, mechanical properties and durability issues were also intensively investigated, in which the significance of activator type and dosage, raw materials' composition, water content and curing conditions [20–24] were highlighted. The recent progress in understanding these blended systems and those modified properties indicates a promising future for the application of alkali activated materials.

On the other hand, limestone powder has been widely utilized in Portland cement systems for the purpose of energy saving and carbon reduction [25]. A maximum limestone replacement of 35 wt.% in Europe is allowed according to the standard EN 197-1 [26]. Beside the environmental benefits, limestone has also been known to improve the workability and strength by the filler effect [27], to accelerate the hydration of C_3S by providing nucleation sites [28], to partly participate in the formation of C–S–H gels [29] and to interact with aluminate-containing phases to form monocarboaluminate [30]. Those studies indicate both physical and chemical modifications of limestone on the Portland cement system. Meanwhile, attention has also been paid to apply this more

* Corresponding author. Tel.: +31 (0)40 247 8225; fax: +31 (0)40 243 8595.
E-mail address: x.gao@tue.nl (X. Gao).

http://dx.doi.org/10.1016/j.cemconcomp.2015.01.007
0958-9465/

sustainable material in alkali activated systems. Moseson et al. [31] incorporated limestone powder into a sodium carbonate activated slag; the optimum synthesizing parameters and some environmental issues were discussed. The reported maximum limestone content was up to 68 wt.%, while the mechanical properties were comparable to Portland cement. Moreover, the carbon emission and energy consumption were reduced by more than 90%. Yip et al. [32] studied the effect of calcite on silicate activated metakaolin, showing that a calcite content of less than 20% benefits the compressive strength; higher contents may lead to disruption of the gel structure. It was suggested that the increase of strength was not only due to the filler effect, as a small amount of released Ca^{2+} from calcite also plays a limited role. Cwirzen et al. [33] investigated the effect of limestone on sodium hydroxide activated metakaolin, showing that limestone slightly promotes the dissolution of metakaolin, and both activator concentrations and curing temperature significantly affect the leaching equilibriums of Ca, Al and Si. As can be noticed, the previous studies showed the superiority of limestone powder addition in sustainable development and mechanical properties, as well as its reactive potential in alkali activated low calcium system. However, there are limited mechanism studies concerning the role of limestone powder in the blended alkaline system (Na_2O–CaO–Al_2O_3–SiO_2), where large amounts of reactive calcium, silica and alumina units are present simultaneously, generated gels of different types are coexistent, and the synthesizing parameters and curing conditions exhibit a more sensitive influence on the final performance.

The purpose of this study is to understand the influence of limestone powder on fresh behavior, early age reaction kinetics, mechanical properties and reaction products of alkali activated blended systems. Ground granulated blast furnace slag and class F fly ash are chosen as solid raw materials due to their worldwide availability, while ambient temperature curing is used because of its advantage in field applications. Both paste and mortar samples are produced and analyzed. The flowability and setting times of slag–fly ash–limestone pastes are identified. The micro-scale analyses are carried out by using isothermal calorimetry, thermogravimetry/differential scanning calorimetry (TG/DSC), X-ray diffraction (XRD) and Fourier transform infrared spectroscopy (FTIR). The potential physical and/or chemical effects of limestone on the blended alkaline system are discussed.

2. Experiment

2.1. Materials

The solid materials used in this study were ground granulated blast furnace slag (GGBS, provided by ENCI B.V., the Netherlands), Class F fly ash and limestone powder. Their chemical compositions were analyzed by X-ray fluorescence and are shown in Table 1. The median particle size (d50) is 12.43 μm for slag, 22.06 μm for fly ash and 10.12 μm for limestone powder. The specific density (kg/m^3) of the used slag, fly ash and limestone powder are 2930, 2300 and 2710, respectively. The detailed particle size distributions, measured applying a light scattering technique using a Master 2000 particle size analyzer, are given in Fig. 1. CEN standard sand in accordance with EN 196-1 [34] was used for the mortar mixes. The activator used was a mixture of sodium hydroxide pellets (analytical level) and sodium silicate solution. The sodium silicate solution has a composition of 27.69% SiO_2, 8.39% Na_2O and 63.92% H_2O by mass. The desired activator modulus (Ms, SiO_2/Na_2O molar ratio) was achieved by adding the appropriate amount of sodium hydroxide pellets into the sodium silicate solution. The mixed activator solution was cooled down to room temperature prior to further use. Distilled water was added in order to reach the desired water/binder ratios.

Table 1
Major chemical compositions of raw materials.

Oxides (wt.%)	Fly ash	GGBS	Limestone
SiO_2	54.6	34.4	0.84
Al_2O_3	24.4	13.3	0.24
CaO	4.44	37.4	53.96
MgO	1.43	9.89	1.01
Fe_2O_3	7.2	0.47	0.32
Na_2O	0.73	0.34	0.21
K_2O	1.75	0.47	0.34
SO_3	0.46	1.23	–
LOI	2.80	1.65	43.01

2.2. Sample preparation

The activator used in this study has an equivalent sodium oxide (Na_2O) content of 5.7% by mass of the solid material and an activator modulus (Ms) of 1.4 for all mixes, determined based on the preliminary study, which would provide sufficient alkalinity without efflorescence. The target activator modulus was reached by mixing the sodium silicate solution and sodium hydroxide pellets with a solution/pellets mass ratio of 6.42. Three levels of slag content (60%, 50% and 40% by mass) and limestone powder additions from 0% to 30% by mass were used. The water/binder ratio by mass was 0.35 for pastes and 0.45 for mortar specimens, the water consisted of the added distilled water and the water contained in the sodium silicate solution. The binder/sand ratio was 3.0 for all mortar samples. The detailed information of the mixture proportions is listed in Table 2. The samples were prepared in a laboratory mixer; the solid raw materials were added into the mixer followed by the activating solution, then the standard sands. The mixtures were mixed at a slow speed for 30 s, then rested for 30 s before another 120 s at a medium speed. The fresh paste/mortar was poured into plastic molds of 40 × 40 × 160 mm^3 and vibrated for 1 min, then covered with a plastic film on the top surface for 24 h; finally all specimens were demolded and cured at a temperature of 20 °C and a relative humidity of 95% until their testing age.

2.3. Testing methods

The workability of the pastes and mortars were evaluated by the flow table tests according to EN 1015-3 [35]. The fresh samples were transferred into a standard conical ring and a free flow without jolting was allowed. Two diameters that are perpendicular to each other were determined and the mean value was recorded as

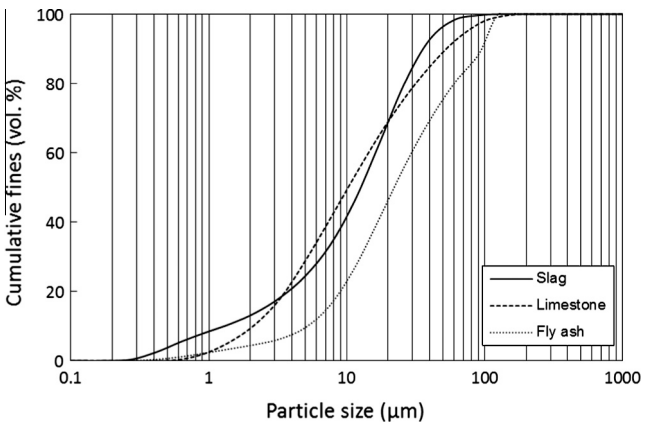

Fig. 1. Particle size distributions of raw materials.

Table 2
Mix proportions of alkali activated slag–fly ash–limestone composites.

	Activator	Solid raw materials			Sand (g)	w/b
		Slag (wt.%)	Fly ash (wt.%)	Limestone (wt.%)		
S60F40L0		60	40			
S50F50L0		50	50	0		
S40F60L0		40	60			
S60F30L10		60	30		0	0.35
S50F40L10		50	40	10	(paste)	(paste)
S40F501L0	Na_2O: 5.7%	40	50			
S60F20L20		60	20			
S50F30L20	Ms: 1.4	50	30	20	300	0.45
S40F40L20		40	40		(mortar)	(mortar)
S60F10L30		60	10			
S50F20L30		50	20	30		
S40F30L30		40	30			

the slump flow. The initial and final setting times were measured by the Vicat needle method as described in EN 196-3 [36]. The determined values were an average of three samples.

The reaction kinetics was studied by an isothermal calorimeter (TAM Air, Thermometric). The solid raw materials were firstly mixed with the activating solution externally for about 1 min and vibrated with an electrical vibrator, then the mixed paste was injected into an sealed glass ampoule and loaded into the calorimeter. All measurements were conducted for 72 h under a constant temperature of 20 °C. The heat release and heat flow results were normalized by mass (g) of binder, the binder includes the solid raw materials and the solid contents in the activator solution.

The compressive strength tests were carried out according to EN 196-1. Cube samples with a size of $40 \times 40 \times 40\ mm^3$ were prepared and tested at the ages of 7 and 28 d, and the strength value for each sample was obtained from an average of six specimens.

The thermo-gravimetric and differential scanning calorimetry (TG/DSC) analysis was conducted in a STA 449 F1 instrument, ground powder samples after 28 d of curing were heated up to 1000 °C at a rate of 10 °C/min with nitrogen as the carrier gas. The temperature was held at 105 °C for 2 h during the heating process.

The Fourier transform infrared spectroscopy (FTIR) measurement was performed in a Varian 3100 instrument with the wavenumbers ranging from 4000 to 650 cm^{-1} at a resolution of 1 cm^{-1}. The X-ray diffraction (XRD) analysis was carried out with a step size of 0.02° and a 2θ range from 10° to 80°. Both the FTIR and XRD analysis were carried out on samples at the age of 28 d.

3. Results and discussion

3.1. Flowability

The slump flow of the fresh alkali activated slag–fly ash–limestone pastes is presented in Fig. 2. The data briefly illustrates the relationships between the raw materials' composition and the workability of the blended pastes. All samples show satisfying flowabilities that range from 29.3 to 33.5 cm. For samples without limestone powder addition, the slump flow increases from 29.3 to 31.4 cm when the slag content decreases from 60% to 40%. A similar tendency is also found in samples with a constant limestone powder replacement, namely that a lower slag content exhibits a better flowability. This is in agreement with previous studies that indicated that alkali activated fly ash shows better workability than slag [37,38] and a higher fly ash content in the slag/fly ash mixes leads to an improvement of flowability [39,40]. This

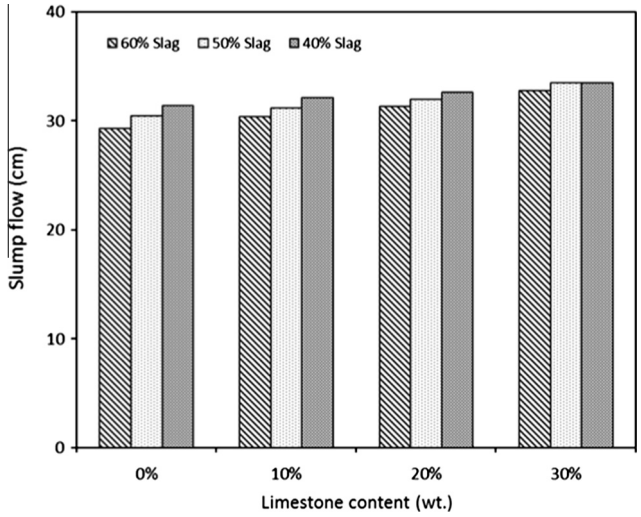

Fig. 2. Slump flow of AA–slag–fly ash–limestone pastes with a w/b of 0.35.

phenomenon can be explained by the higher water demand of slag caused by its angular particle shape and larger surface area compared to fly ash. Besides, the addition of limestone powder also exhibits a positive effect on flowability. It can be seen that in samples with a constant slag content, the slump flow increases with the increasing limestone content in all cases. Moreover, the influence of the slag content on workability seems to be weakened when a higher limestone content is used. It should be noted that for a constant slag content, the increased limestone replacement will also lead to the reduction of fly ash content in the slag–fly ash–limestone ternary blends. The improved flowability in samples with higher limestone contents may imply that the limestone powder presents a better flowability in alkali solutions than fly ash in this case. Another possible explanation for the improved flowability is that the particle packing of the paste also affects the water demand. By using fine limestone powders in slag and fly ash mixes, more fine particles with relatively low water demand will be filled in the micro voids, then a better particle packing is achieved; therefore, more available water can be provided to lubricate the particles resulting in a higher slump flow [41,42]. In terms of the mortar mixtures, a higher water/binder ratio of 0.45 was used in order to meet the water demand of the fine aggregates. The relations between the binder composition and the slump flow for mortars is depicted in Fig. 3. All mixes show ideal slump flows between 23.2 and 27.4 cm without jolting, with no segregation observed. Similar to the results of paste samples, the workability is improved when lowering the slag content and/or increasing the limestone content.

3.2. Setting times

Fig. 4 depicts the influence of the starting materials' composition on the initial and final setting times of alkali activated slag–fly ash–limestone blends. It can be seen that both the initial and final settings are retarded when lowering the slag content. For instance, the mixtures with a slag content of 60% show an initial setting time of 45 min, which increases to 55 and 68 min when the slag content is reduced to 50% and 40%, respectively. Similarly, the final setting time increases from 93 min to 115 min as the slag content decreases from 60% to 40%. The previous studies also show that a higher slag content in the alkali activated slag–fly ash mixes results in decreased setting times [20,43]. The significant influence of slag on setting times is attributed to its high reactivity under alkali conditions, as the relatively fast dissolution rate of Ca,

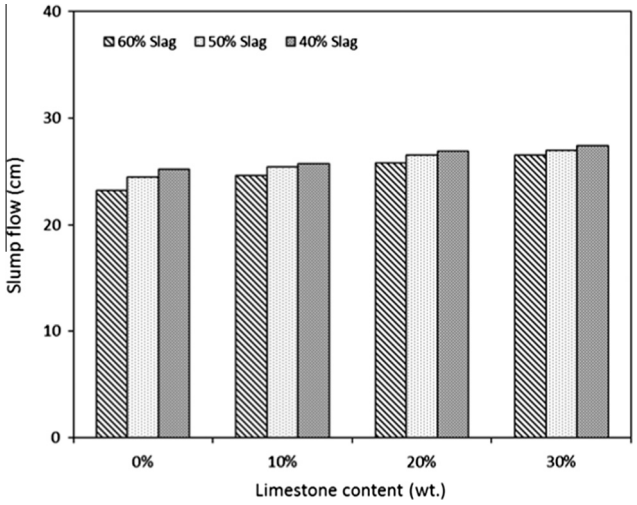

Fig. 3. Slump flow of AA-slag–fly ash–limestone mortars with a w/b of 0.45.

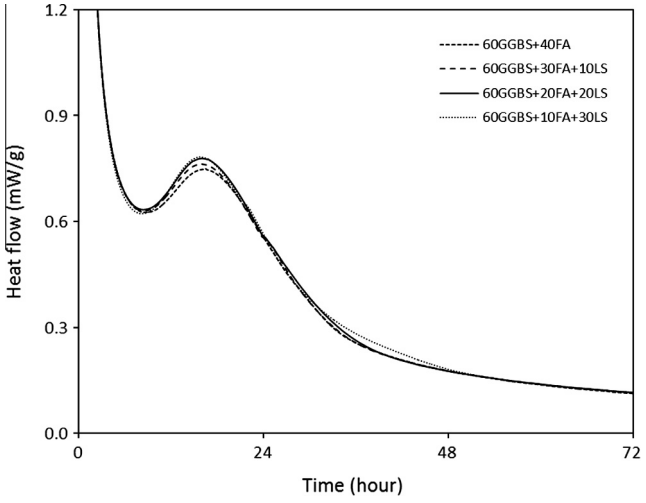

Fig. 5. Normalized heat flow of AA slag–fly ash–limestone pastes with 60% Slag.

Si and Al units from the slag and the higher total amount of those units (especially Ca) that are present in the solution accelerate the formation rate of reaction products and the setting processes. On the other hand, for a constant slag content, it can be concluded that the influence of limestone and fly ash proportion on the initial and final setting times is negligible, since the variations in the initial and final setting times caused by the composition changes of limestone and fly ash are within only 3 min in all cases. It also implies that the fly ash exhibits similar and very low reactivity as limestone powder during the initial stage of reaction. Thus from the angle of the raw material composition, the slag content appears to be the only key factor that influences the setting behaviors of the alkali activated slag–fly ash–limestone blends cured under ambient temperature.

3.3. Reaction kinetics

The normalized heat flow of alkali activated slag–fly ash–limestone blends (with a slag content of 60% and limestone addition from 0% to 30%) within the first 72 h are shown in Fig. 5. The presented calorimetric curves are in accordance with the previous studies on silicate activated slag or its mixtures [44–46], which show four typical reaction stages including initial dissolution, induction, acceleration/deceleration and a stable period. The initial dissolution stage corresponds to the initial wetting and dissolution of the raw materials. It usually occurs within the first few minutes of mixing [47] and is generally regarded as a physical process, although some chemical reactions are possibly involved. The calorimetric peaks of this stage are not shown in the figure due to its much higher magnitude. The acceleration peak is located at around 16 h after mixing, which is assigned to the massive formation of reaction products from dissolved Ca, Si and Al units [48]. It can be noticed that as the limestone content increases, the heat evolution peak slightly shifts to earlier locations with higher intensities. It indicates that the reaction process of alkali activated slag–fly ash blends is slightly accelerated in the presence of limestone powder. This is in agreement with previous researches on the effect of limestone powder in Portland cement hydration [28,49]. The incorporation of limestone powder brings more fine particles in the system, which provides additional nucleation sites for the formation and growth of reaction products, then as a result the reaction process is accelerated [50]. It can be seen that the induction period is also slightly shortened with the increasing limestone content. During this stage, the newly formed reaction products cover the surfaces of unreacted particles [51] and temporarily limit the reaction process. Further reaction continues when the alkalis penetrate the covered layers and reach the raw materials again [46]. Considering the induction period is promoted in a limited manner, it is more likely that the acceleration in this stage is due to the micro-nucleation effect of the fine particles from limestone powder and the better dispersion of slag, rather than a chemical process.

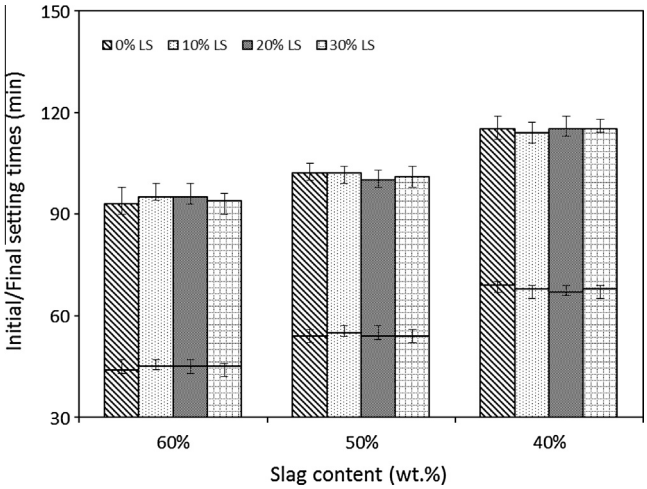

Fig. 4. Setting times of AA-slag–fly ash–limestone pastes.

Fig. 6 illustrates the heat evolution curves of samples with a slag content of 40% and limestone additions up to 30%. It can be noticed that both the induction and acceleration stages are significantly retarded when compared to the mixes shown in Fig. 5. For instance, the induction stage is around 7.5 h in samples with a slag content of 60%, while it shifts to approximately 11 h when the slag content decreases to 40%, also a considerably prolonged induction time and reduced heat flow can be observed. Similarly, when lowering the slag content from 60% to 40%, the acceleration peak shifts from about 16 to 20 h with a decreased peak intensity from about 0.8 to 0.5 mW/g. Those changes demonstrate the remarkable effects of the slag content on the early age reaction. The glassy structure of slag is mainly formed by Si and Al cations, and the Ca cation works as a network modifier [6]. Under alkali activation, the breakdown of a calcium enriched structure is easier than Si and

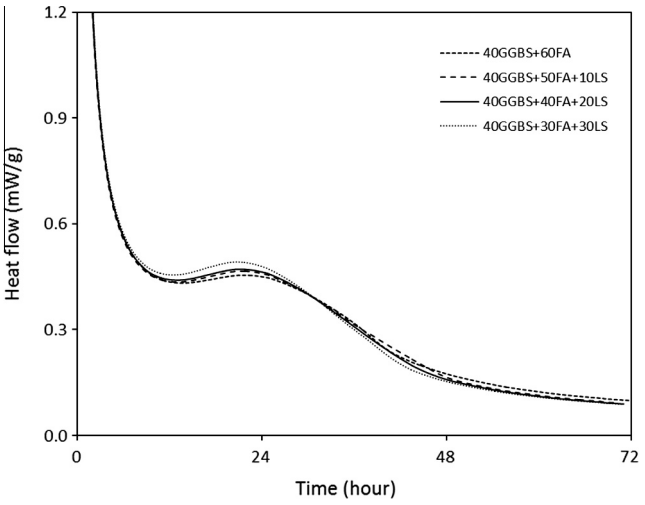

Fig. 6. Normalized heat flow of AA slag–fly ash–limestone pastes with 40% Slag.

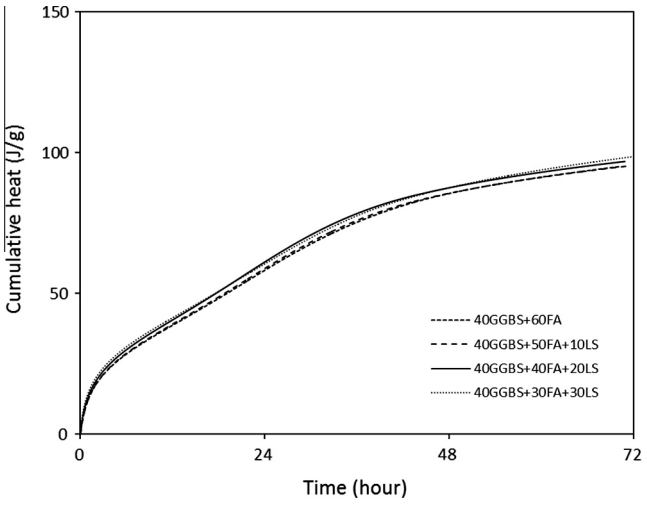

Fig. 8. Cumulative heat release of AA slag–fly ash–limestone pastes with 40% Slag.

Al dominated structures such as fly ash. This phenomenon is more significant at ambient temperature. Thus, a higher slag content will lead to a larger amount of available Si, Al and Ca units in solution, and consequently a more intense dissolution and reaction process. Similar to the results shown in Fig. 5, an evident promotion in induction and acceleration stage due to the increase of limestone powder content is observed. But compared to the significant changes caused by slag, the effect of limestone powder on the early age hydration is at a relatively small scale. Figs. 7 and 8 show the cumulative heat evolution of different slag–fly ash–limestone mixes. The first dramatic increase is associated with the initial wetting and dissolution of raw materials in alkaline solution; the following relatively moderate increase corresponds to the induction stage; the second sharp increase is assigned to the acceleration stage. It can be seen that for a constant slag content, samples with a higher limestone content exhibit a higher total heat release, indicating the presence of limestone powder benefits the reaction process within the tested 72 h; while for samples with a constant limestone content, higher slag contents exhibit considerably higher total heat release, which implies again that a more significant influence of slag than limestone/fly ash on the reaction in early stage.

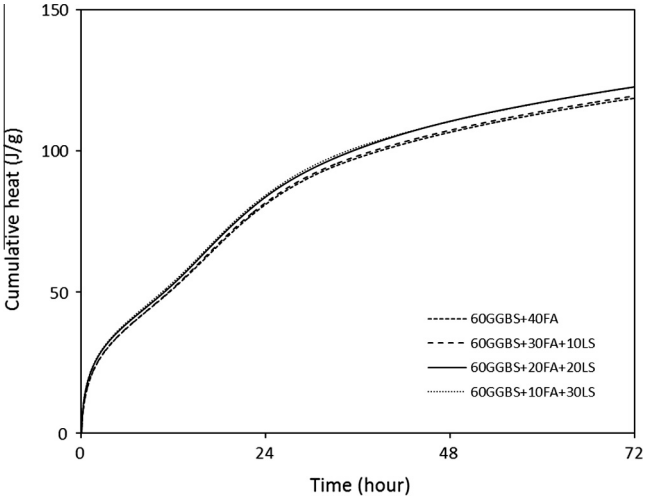

Fig. 7. Cumulative heat release of AA slag–fly ash–limestone pastes with 60% Slag.

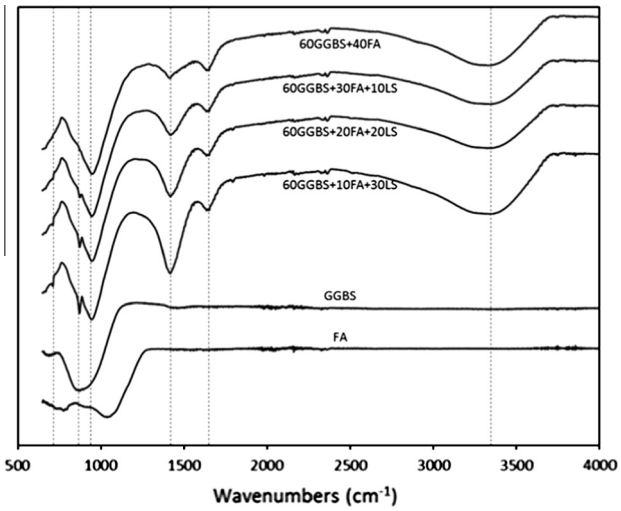

Fig. 9. FTIR spectra of slag, fly ash and alkali activated slag–fly ash–limestone pastes.

3.4. FTIR and XRD analysis

Fig. 9 shows the infrared spectra of the unreacted slag, fly ash and slag–fly ash–limestone blends after alkali activation. The main vibration band is at around 900 cm^{-1} for slag and about 1020 cm^{-1} for fly ash, which are associated with the asymmetric stretching vibration of terminal Si–O and bridge Si–O–T bonds, respectively [52,53]. The difference in the main absorption band illustrates the different glassy networks of the raw materials. The absorption bands located at around 1080, and 600–800 cm^{-1} in fly ash indicates the presence of quartz and mullite [54]. After alkali activation, all mixes showed OH groups at 1640 cm^{-1} and around 3350 cm^{-1}, demonstrating the presence of chemically bound water within the reaction products [55]. The absorption bands at around 1420, 870 and 710 cm^{-1} correspond to the vibrations of O–C–O in carbonates [23]. The main absorption band of the reaction products is located at around at 950 cm^{-1} in all mixes, which is assigned to the asymmetric stretching vibration of Si–O terminal (non-bridging) bonds, indicating that the main reaction product is a chain structured C–A–S–H type gel. The Si–O bond in unreacted slag is around 900 cm^{-1}; the shifting of this band to higher wavenumbers implies the formation of a more highly polymerized Si–O network,

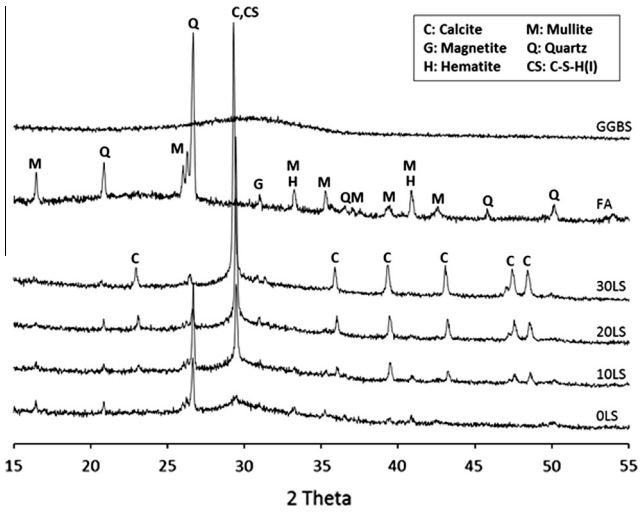

Fig. 10. XRD patterns of slag, fly ash and alkali activated slag–fly ash–limestone pastes.

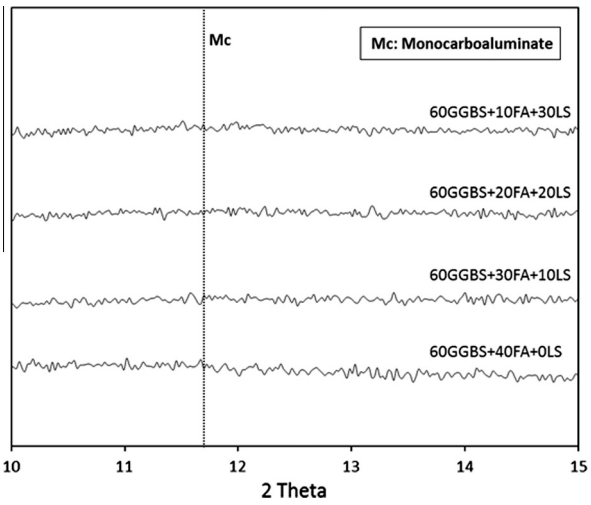

Fig. 11. XRD patterns of alkali activated slag–fly ash–limestone pastes at low angles.

namely the occurrence of the polymerization process. Concerning the fly ash, the main absorption bands shifts from 1020 cm^{-1} to lower numbers after activation, indicating that the high crosslinking networks with bridging Si–O bonds are not formed in this study. This is probably due to the presence of a large amount of calcium at early stages, which consume the Si and Al units and preferably form C–A–S–H type gels, so that the accumulation of Si, Al units is hindered. It can be seen that as the limestone content increases, the intensity of the absorption bands that represent carbonates increase significantly; while compared to the changes in O–C–O groups, no remarkable change is observed in the absorption bands (both location and intensity) of bound water and terminal Si–O. It may demonstrate that the presence of limestone powder shows inconspicuous influence on the gel structure of alkali activated slag–fly ash blends. Since the FTIR spectra provide limited information on quantitative determination, a TG/DSC analysis was carried out and the results are presented later in this paper to identify the gel composition in detail.

The XRD patterns of unreacted slag and fly ash are shown in Fig. 10, as well as the samples with a slag content of 60% and limestone additions from 0% to 30%. It can be seen that the original slag is mainly amorphous without significant crystalline phases, and shows a peak hump between 25° and 35° due to the amorphous components; while the unreacted fly ash contains crystalline phases such as quartz (SiO_2), mullite ($Al_6Si_2O_{13}$), maghemite and hematite (Fe_2O_3) with a broad amorphous hump between 15° and 30°. Similar to the FTIR results, the differences in the location of the amorphous hump indicate the structural differences between the slag and fly ash. After activation, the characteristic peaks of quartz, mullite and maghemite/hematite from fly ash remain. The incorporation of limestone leads to the presence of calcite peaks. The intensity changes of those crystalline peaks in the reaction products are due to the different relative contents of fly ash and limestone in each mixture. All samples show a main reaction product at around 29.5°, which is identified as a poorly crystallized C–(A)–S–H gel (type I, PDF#00-034-0002). This is in accordance with the FTIR analysis that the main reaction product is characterized by terminal Si–O bonds and chain structure. Besides, no significant newly formed crystalline phases are observed until the age of 28 d and the reaction products remain amorphous. As can be noticed, there is no significant change in the intensity and location of C–(A)–S–H peaks when the slag content is kept constant, implying the limited influence of both limestone powder and fly ash content on the gel structure of the main reaction products until the age of 28 d.

In addition, previous studies concluded that the presence of limestone powder would lead to the formation of monocarboaluminate in both Portland cement and alkali activated systems, especially in high aluminate conditions (i.e. high C_3A, C_4AF content; fly ash/metakaolin addition), and the formation of those phases are detectable after 28 d of curing [27,33,56–58]. In order to identify whether this phase is formed in silicate activated slag–fly ash–limestone blends, an XRD observation that focused on low angles was conducted and the result is shown in Fig. 11. It can be seen that the characteristic peak of monocarboaluminate, which is usually shown at around 11.7° [59], is not observed in this study. Thus, it can be concluded that no evident chemical reaction took place between the limestone powder and the aluminate units in this case, or the chemical reactions involving the limestone powder did not result in the formation of additional crystalline phases.

3.5. TG/DSC analysis

The thermogravimetry results of samples with a slag content of 60% and limestone additions up to 30% are presented in Fig. 12. All samples exhibit a remarkable mass loss before around 110 °C, which is assigned to the loss of physically bound water within the paste [60]. Specimens without limestone show an evaporable water content of 16.1%, which is slightly lower than the ones with limestone addition, but there is no further increase in this value when increasing the limestone content from 10% to 30%. After the evaporation of the physically bound water, all samples show a negligible mass loss between 105 and 180 °C, followed by a gradual decrease in mass until heated to around 600 °C. The gradual and continuous mass loss after around 180 °C is attributed to the decomposition of the C–(A)–S–H type gels. After around 600 °C, mixes without limestone powder show a stable curve with only a slight mass loss until 1000 °C, and no other abrupt mass losses are observed between 105 and 1000 °C. This reveals that the reaction products are mainly amorphous gels with bound water. When the limestone powder is incorporated, samples show a remarkable mass loss between 600 and 800 °C, which is mainly caused by the decomposition of the calcium carbonates [61].

The corresponding differential scanning calorimetry (DSC) results are depicted in Fig. 13. The heat absorption peak at around 110 °C is associated with the evaporation of the physically bound water. The smooth absorption peak at around 180 °C indicates

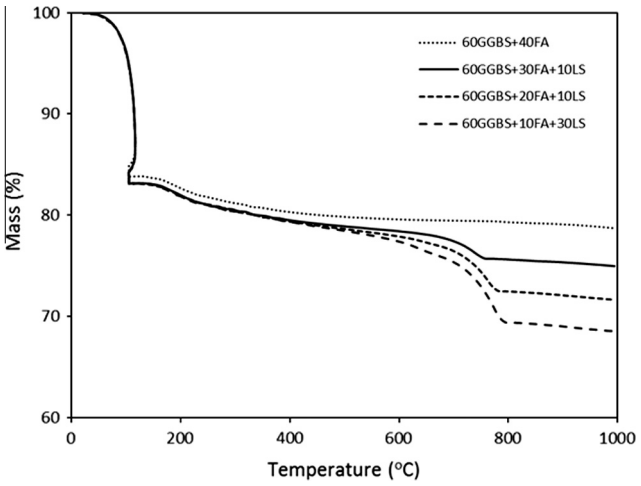

Fig. 12. TG analysis of alkali activated slag–fly ash–limestone pastes.

the decomposition of the reaction products [62], then the gradual decomposition processes including the loss of chemically bound water take place. It can be seen that as the limestone powder content increases, the heat absorption peak at around 750 °C becomes more significant, representing a more intensive decomposition process due to the higher content of calcium carbonate. It should be noted that all samples also show an exothermic peak at around 800 °C, while no remarkable changes are observed in TG analysis at the same temperature. This heat release peak is attributed to the formation of more ordered crystalline phases under high temperature, which was also found in a previous study concerning alkali activated slag [62].

Based on the understandings above, a calculation on the physically and chemically bound water contents was carried out in order to study the effect of limestone powder on the composition of the reaction products. The physically bound water content was calculated as the mass loss before 105 °C; the chemically bound water content in each mix is calculated by the mass loss between 105 °C and 1000 °C, with the exclusion of the mass loss due to the incorporated limestone. The mass loss of limestone between 105 °C and 1000 °C is 43.01% according to the TG analysis, this value includes the mass loss of calcium carbonate and the impurities from limestone powder; the calculated total mass includes the alkali activator and solid raw materials. The results are presented

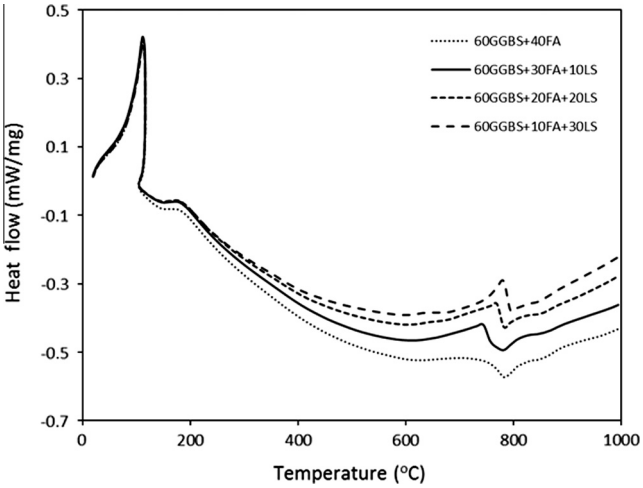

Fig. 13. DSC analysis of alkali activated slag–fly ash–limestone pastes.

in Table 3, where it can be seen that the addition of limestone powder leads to a slight increase in the total chemical water content. This phenomenon can be partly explained by the XRD results in this study that the addition of limestone powder does not evidently lead to the formation of additional reaction products, thus no remarkable amount of extra bound water can be observed. However, it is possible that the additional nucleation sites that are provided by the fine limestone particles promote the formation of hydrated gels and refine the pore structures, then result in slightly increased physically and chemically bound water contents; or a slight but non-ignorable amount of Ca^{2+} is released from the fine limestone particles under alkali activation, then participates in the reaction process and leads to a slight increase in the bound water content.

3.6. Compressive strength

The 7 and 28 d compressive strengths of alkali activated slag–fly ash–limestone pastes and mortars are shown in Figs. 14 and 15, respectively. The water/binder ratio for paste samples is 0.35, and it is 0.45 for mortars. It can be seen that the paste and mortar samples show a similar tendency in the strength development, and mortar mixtures exhibit a lower strength in general, due to their increased water content.

For samples with a constant slag content, both the 7 and 28 d compressive strengths are increased when increasing the limestone powder content. For instance, in the paste samples with a slag content of 60%, when increasing the limestone powder content from 0% to 30%, the 7 d compressive strength increases from 61.3 MPa to 68.9 MPa, and the 28 d strength also exhibits an increment from 76.5 MPa to 83.5 MPa. Similar results are also found in samples with other slag contents and the highest strength is shown in samples with the 30% limestone addition. This behavior should be attributed to the filler effect of limestone powder. The addition of limestone powder will lead to a higher content of fine particles within the paste (see Fig. 1), which could work as micro aggregates and may reduce the total porosity, then result in an increment of strength. Moreover, the better reaction of slag due to the presence of limestone also contributes to the strength improvement. Since the additional nuclear sites provided by the fine limestone particles promote the formation of the reaction products, as can be seen from the isothermal calorimeter results, a more homogeneous dispersion of the reaction products may result. The improved slump flow caused by the limestone addition could be an indication of the increased effective water content, which may result in an increase of the contact area between the slag particles and alkaline solutions.

It can be obviously seen that for a constant limestone replacement, higher compressive strengths are achieved in samples with higher slag contents at both 7 and 28 d. As shown in Fig. 14, for samples without limestone addition, when reducing the slag content from 60% to 40%, the 7 d compressive strength decreases from 61.3 MPa to 44.8 MPa and the 28 d strength is reduced from 76.5 MPa to 56.3 MPa. Similarly, in samples with a 30% limestone

Table 3
Calculation of bound water content (wt.%).

	60GGBS 40FA 0LS	60GGBS 30FA 10LS	60GGBS 20FA 20LS	60GGBS 10FA 30LS
Mass loss between 105–1000 °C	5.09	8.11	11.46	14.53
Limestone powder incorporated	0	6.70	13.38	20.07
Mass loss of limestone powder	0	2.88	5.75	8.64
Chemical bound water	5.09	5.23	5.71	5.89
Physical bound water	16.1	16.9	16.9	16.9

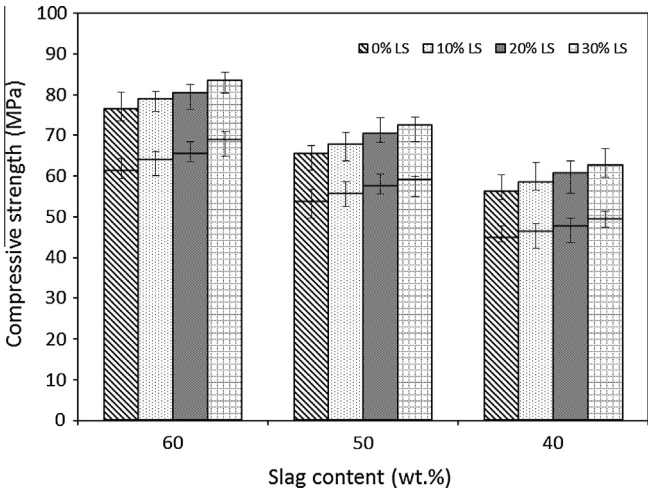

Fig. 14. 7 and 28 days compressive strength of AA-slag–fly ash–limestone pastes.

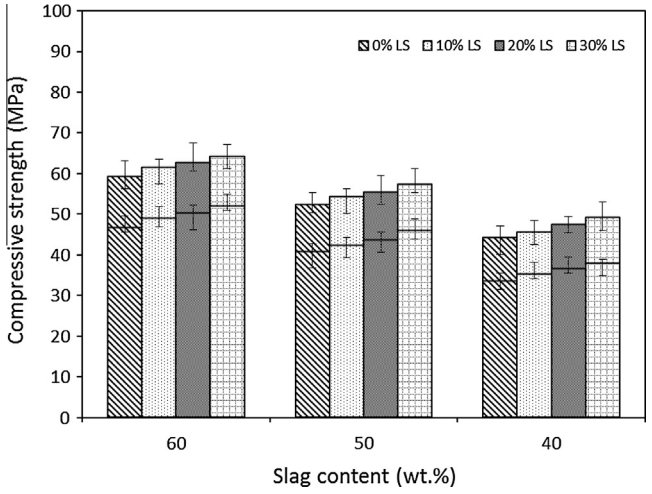

Fig. 15. 7 and 28 days compressive strength of AA-slag–fly ash–limestone mortars.

content, where the highest strength is achieved in each slag level, the 7/28 d strength decreases from 68.9/83.5 MPa to 49.4/62.7 MPa respectively, with the shifting of the slag content from 60% to 40%. The significant influence of the slag content on mechanical strength was also reported in previous studies [20,63,64]. This should be attributed to the considerably higher reactivity of slag than the other components under ambient temperature. As can be seen from the results of the setting times and the reaction kinetics, the slag content shows a decisive impact on the reaction process, while changing the limestone/fly ash content based on a constant slag level exhibits limited influences. In addition, the FTIR and XRD analyses show that the main reaction product in these ternary blends is a typical hydrated gel of alkali activated slag [7], which again indicates the dominant role of slag. Therefore, a higher slag content will result in a more intensive reaction process and a higher amount of reaction products, namely a higher compressive strength. It can be noted that based on a constant slag content, mixes with different limestone contents show a similar rate of strength development between the 7 and 28 d. Considering that the increased limestone content is at the expense of fly ash content in this case, it also demonstrates the low reactivity of fly ash until the age of 28 d under ambient curing conditions; or the dissolved Si and Al units from fly ash exhibits much less influence than the Ca from slag on strength in this case.

Concerning the mortar mixes, the filler effect of limestone powder and the remarkable influence of slag on strength are also obviously presented. As shown in Fig. 15, based on a constant slag level, the compressive strength increases with the increasing limestone content; also based on a constant limestone addition, both the 7 and 28 d strength increase with the increasing slag content. The highest values are obtained in samples with a 60% slag and 30% limestone, showing 7 and 28 d compressive strengths of 51.9 MPa and 64.2 MPa, respectively. While the lowest 7/28 d strength of 46.6/59.2 MPa was shown in samples with 40% slag and 0% limestone.

3.7. The role of limestone powder in blended alkali systems

As commonly known, limestone powder exhibits both physical and chemical effects on Portland cement systems, which can be briefly summarized as follows: lowering the water demand of cement paste [65]; accelerating the hydration process; reacting with aluminate phases to form hemicarbonate and monocarboaluminate [66] and affecting the strength. While in an alkali activated system, according to the investigations in this paper, the physical effect of limestone powder is obvious. As shown in the slump flow results, the low water demand of limestone powder promotes the workability of both pastes and mortars. Moreover, owing to the fine particles provided by the limestone powder, the reaction process is slightly accelerated; the higher intensities of the acceleration peak and the higher total heat release indicate an intensified reaction. The increment in compressive strength can also be attributed to the physical modification of limestone powder, as fine particles from the limestone powder modify the packing and result in a denser matrix.

However, the chemical effects of limestone powder in the blended alkali system are different from those in a Portland cement system. It has been known that the presence of limestone in calcium and high aluminates conditions modifies the Portland cement system following the mechanism expressed as:

$$A + 3CH + 8H + C\underline{C} \Rightarrow C_4A\underline{C}H_{11} \quad (1)$$

where $A = Al_2O_3$, $CH = Ca(OH)_2$, $H = H_2O$, $C\underline{C} = CaCO_3$.

This process increases the total volume of the solid phases and results in the increment of compressive strength in Portland cement systems. The occurrence of this reaction is highly dependent on the Al and Ca supply, while the limestone powder content and fineness plays a minor role [59,70]. In the case of alkali activated slag–fly ash–limestone blends, all the required elements for the reaction above are available, but the formation of $C_4A\underline{C}H_{11}$ is not observed according to the micro analysis (XRD) in this study. One possible explanation is that the dissolved Ca, Si, Al units from the slag and fly ash prefer the formation of more stable structure of C–(A)–S–H type gels, when the formation of C–(A)–S–H gel is saturated, the remaining units may react with limestone powder to form $C_4A\underline{C}H_{11}$. However, it seems that the remaining components in ternary slag–fly ash–limestone blends do not meet the requirements of the equation above, the possible reasons can be as follows: (1) Absence of calcium. The C–S–H gels in alkali activated system (type I, tobermorite) show a Ca/Si of around 1.0–1.2 [67,71] and the Ca/Si (molar ratio) in the raw slag is 1.17. While the total Ca/Si in the system would be lower than 0.85 (in samples with 60% slag) when calculating the silicate from the activator, this value would be even lower when considering the silicate from fly ash. Thus no sufficient calcium will remain after the formation of C–(A)–S–H gels. (2) Absence of aluminate. It has been proven that the C–(A)–S–H gels in alkali activated systems also have the potential to contain a certain amount of aluminate [68,69], and the total Al/Ca in C–S–H gels can reach around 0.2

[67]. Even though the Al/Ca ratio in original slag reaches 0.17, the dissolution of fly ash at ambient temperature may provide a limited amount of aluminate at early ages. It is also possible that the dissolved aluminate from fly ash may be participating in the formation of low polymerized N–(C)–A–S–H type gels rather than reacting with limestone to form crystalline phases. Therefore, the reaction products of silicate activated slag–fly ash–limestone blends remain amorphous without crystalline phases. But it is still possible for the formation of monocarboaluminate in other alkali systems where additional Ca and Al groups are simultaneously existing, such as systems with high calcium hydroxide and metakaolin/fly ash contents; further investigations on the formation mechanism of monocarboaluminate in alkali activated systems are being carried out. Besides, it should be noted that the dissolution of Ca^{2+} from calcium carbonates in alkali activated system was actually confirmed by [33]; also the satisfying surface binding between the limestone powder and alkali activated materials was suggested in the previous study [32]. Thus, the slightly increased bound water content together with the continuously increased compressive strength (with limestone replacements up to 30%) in this case could be regarded as an indication that the limestone powder may not only work as a non-reactive filler, the release of Ca^{2+} from limestone powder and its topography characteristics may also make small but non-negligible contributions to the strength development and pore structure refinement by providing extra surface binding within particles. Overall, the utilization of extra fine particles (limestone powder) in hybrid alkali systems (alkali activated slag–fly ash blends) exhibits both physical and chemical modifications such as improving workability, promoting reaction processes, and achieving superior compressive strengths with high level limestone replacements.

4. Conclusions

This paper investigates the effects of the raw materials' composition on the workability, setting times, reaction kinetics, gel characteristics and compressive strength of room temperature cured alkali activated slag–fly ash–limestone ternary system. Both paste and mortar mixtures are designed and analyzed, and the role of limestone powder in blended alkali systems is discussed. The following conclusions can be drawn:

- An ideal workability can be achieved in alkali activated slag–fly ash–limestone blends by using high amounts of fly ash and limestone. The flowability improves with the increasing fly ash and limestone powder contents. Both the initial and final setting times are strongly influenced by the slag content, and a higher slag content leads to a decreased setting time; while both fly ash and limestone powder show a negligible influence on setting.
- The additional nucleation sites provided by limestone powder slightly accelerate the induction and acceleration/deceleration stage of reaction and also increase the total heat evolution within the tested 72 h. The slag content plays a dominant role in determining the early age reaction characteristics such as the intensity and location of the typical reaction stages.
- The gel characteristic analyses conducted by FTIR, XRD and TG/DSC show that the reaction products of alkali activated slag–fly ash–limestone blends are governed by the chain structured C–(A)–S–H type gels. The presence of limestone powder does not lead to the formation of new phases, but slightly increases both the physically and chemically bound water content.
- For a constant limestone powder replacement, a higher compressive strength was observed in samples with a higher slag content; while for a constant slag content, the compressive strength increases with an increasing limestone powder content. The slag content exhibits a more significant effect than the other components on strength.
- The limestone powder shows mainly physical with slight but non-ignorable chemical modifications of alkali activated slag–fly ash blends. It is suggested that the absence of monocarboaluminate is due to the insufficient supply of additional calcium and aluminate in this case; and the small amount of the released Ca^{2+} from the limestone together with its filler effect results in the pore refinement and strength increment.

Acknowledgements

This research was supported by China Scholarship Council and the Department of the Built Environment at Eindhoven University of Technology. The authors gratefully thank Mr. P. de Vries (ENCI B.V., the Netherlands) and Mr. J. van Eijk (Knauf Insulation, the Netherlands) for the materials supply. Furthermore, the authors wish to express their gratitude to the following sponsors of the Building Materials research group at TU Eindhoven: Rijkswaterstaat Grote Projecten en Onderhoud; Graniet-Import Benelux; Kijlstra Betonmortel; Struyk Verwo; Attero; Enci; Rijkswaterstaat Zee en Delta-District Noord; Van Gansewinkel Minerals; BTE; V.d. Bosch Beton; Selor; GMB; Geochem Research; Icopal; BN International; Eltomation; Knauf Gips; Hess AAC Systems; Kronos; Joma; CRH Europe Sustainable Concrete Centre; Cement & Beton Centrum; Heros and Inashco (in chronological order of joining).

References

[1] Wang SD, Scrivener KL, Pratt PL. Factors affecting the strength of alkali-activated slag. Cem Concr Res 1994;24(6):1033–43.
[2] Fernández-Jiménez A, García-Lodeiro I, Palomo A. Durable characteristics of alkali activated fly ashes. J Mater Sci 2007;42:3055–65.
[3] Bakharev T, Sanjayan JG, Cheng YB. Resistance of alkali-activated slag concrete to acid attack. Cem Concr Res 2003;33:1607–11.
[4] Hai YZ, Venkatesh Kodur, Shu LQ, Liang C, Bo W. Development of metakaolin–fly ash based geopolymers for fire resistance applications. Constr Build Mater 2014;55:38–45.
[5] Puertas F, Fernández-Jiménez A. Mineralogical and microstructural characterisation of alkali-activated fly ash/slag pastes. Cem Concr Compos 2003;25:287–92.
[6] Chao Li, Henghu Sun, Longtu Li. A review: the comparison between alkali-activated slag (Si+Ca) and metakaolin (Si+Al) cements. Cem Concr Res 2010;40:1341–9.
[7] Brough AR, Atkinson A. Sodium silicate-based alkali-activated slag mortars: Part I. Strength, hydration and microstructure. Cem Concr Res 2002;32:865–79.
[8] Granizo ML, Alonso S, Blanco-Varela MT, Palomo A. Alkaline activation of metakaolin: effect of calcium hydroxide in the products of reaction. J Am Ceram Soc 2002;85(1):225–31.
[9] Palacios M, Puertas F. Effect of shrinkage-reducing admixtures on the properties of alkali-activated slag mortars and pastes. Cem Concr Res 2007;37:691–2.
[10] Fernández-Jiménez A, Puertas F. Setting of alkali-activated slag cements influence of activator nature. Adv Cem Res 2001;13(3):115–21.
[11] Bakharev T. Thermal behaviour of geopolymers prepared using class F fly ash and elevated temperature curing. Cem Concr Res 2006;36:1134–47.
[12] Rashad Alaa M. A comprehensive overview about the influence of different admixtures and additives on the properties of alkali-activated fly ash. Mater Des 2014;53:1005–25.
[13] Lee NK, Lee HK. Setting and mechanical properties of alkali-activated fly ash/slag concrete manufactured at room temperature. Constr Build Mater 2013;47:1201–9.
[14] Rashad Alaa M. Properties of alkali-activated fly ash concrete blended with slag. Iran J Mater Sci Eng 2013;10(1):57–64.
[15] Aydin S. A ternary optimization of mineral additives of alkali activated cement mortars. Constr Build Mater 2013;43:131–8.
[16] Sugama T, Brothers LE, Van de Putte TR. Acid-resistant cements for geothermal wells: sodium silicate activated slag/fly ash blends. Adv Cem Res 2005;17(2):65–75.
[17] Yip CK, Lukey GC, van Deventer JSJ. The coexistence of geopolymeric gel and calcium silicate hydrate at the early stage of alkaline activation. Cem Concr Res 2005;35:1688–97.

[18] García-Lodeiro I, Macphee DE, Palomo A, Fernández-Jiménez A. Effect on fresh C–S–H gels the simultaneous addition of alkali and aluminium. Cem Concr Res 2010;40:27–32.
[19] Ismail I, Bernal SA, Provis JL, Nicolas RS, Hamdan S, Deventer JSJ. Modification of phase evolution in alkali-activated blast furnace slag by the incorporation of fly ash. Cem Concr Compos 2014;45:125–35.
[20] Kumar S, Kumar R, Mehrotra SP. Influence of granulated blast furnace slag on the reaction, structure and properties of fly ash based geopolymer. J Mater Sci 2010;45(3):607–15.
[21] Chi M, Huang R. Binding mechanism and properties of alkali-activated fly ash/slag mortars. Constr Build Mater 2013;40:291–8.
[22] Puertas F, Martínez-Ramírez S, Alonso S, Vázquez E. Alkali-activated fly ash/slag cement. Strength behaviour and hydration products. Cem Concr Res 2000;30:1625–32.
[23] Bernal SA, Provis JL, Rose V, Mejía de Gutierrez A. Evolution of binder structure in sodium silicate-activated slag-metakaolin blends. Cem Concr Compos 2011;33:46–54.
[24] Bernal SA, Mejía de Gutierrez A, Provis JL. Engineering and durability properties of concretes based on alkali-activated granulated blast furnace slag/metakaolin blends. Constr Build Mater 2012;33:99–108.
[25] Yilmaz B, Olgun A. Studies on cement and mortar containing low-calcium fly ash, limestone, and dolomitic limestone. Cem Concr Compos 2008;30(3):194–201.
[26] BS EN 197-1:2011. Cement. Composition, specifications and conformity criteria for common cements.
[27] Antonia M, Rossena J, Martirena F, Scrivener K. Cement substitution by a combination of metakaolin and limestone. Cem Concr Res 2012;42:1579–89.
[28] Tyditat V, Matas T, Cerny R. Effect of w/c and temperature on the early-stage hydration heat development in Portland-limestone cement. Constr Build Mater 2014;50:140–7.
[29] Kakali G, Tsivilis S, Aggeli E, Bati M. Hydration products of C_3A, C_3S and Portland cement in the presence of $CaCO_3$. Cem Concr Res 2000;30:1073–7.
[30] Bonavetti VL, Rahhal VF, Irassar EF. Studies on the carboaluminate formation in limestone filler-blended cements. Cem Concr Res 2001;31:853–9.
[31] Moseson AJ, Moseson DE, Barsoum MW. High volume limestone alkali - activated cement developed by design of experiment. Cem Concr Compos 2012;34(3):328–36.
[32] Yip CK, Provis JL, Lukey GC, Deventer JSJ. Carbonate mineral addition to metakaolin-based geopolymers. Cem Concr Compos 2008;30(3):979–85.
[33] Cwirzen A, Provis JL, Penttala V, Cwirzen KH. The effect of limestone on sodium hydroxide-activated metakaolin-based geopolymers. Constr Build Mater 2014;66:53–62.
[34] British standard EN 196-1:2005. Methods of testing cement Part 1: determination of strength.
[35] British standard EN 1015-3:1999. Methods of test for mortar for masonry Part 3: determination of consistence of fresh mortar.
[36] British standard EN 196-3:2005. Methods of testing cement Part 3: determination of setting times and soundness.
[37] Yang KH, Song JK, Lee KS, Ashrour AF. Flow and compressive strength of alkali-activated mortars. ACI Mater J 2009;106:50–8.
[38] Yang KH, Song JK, Ashour AF, Lee ET. Properties of cementless mortars activated by sodium silicate. Construct Build Mater 2008;22:1981–9.
[39] Nath P, Sarker PK. Effect of GGBFS on setting, workability and early strength properties of fly ash geopolymer concrete cured in ambient condition. Construct Build Mater 2014;66:163–71.
[40] Deb PS, Nath P, Sarker PK. The effects of ground granulated blast-furnace slag blending with fly ash and activator content on the workability and strength properties of geopolymer concrete cured at ambient temperature. Mater Des 2014;62:32–9.
[41] Yu QL, Spiesz P, Brouwers HJH. Development of cement-based lightweight composites – Part 1: mix design methodology and hardened properties. Cem Concr Compos 2013;44:17–29.
[42] Yu QL. Design of environmentally friendly calcium sulfate-based building materials, Ph.D. Thesis, Eindhoven University of Technology, The Netherlands; 2010. p. 1–208.
[43] Ismail I, Bernal SA, Provis JL, Hamdan S, van Deventer JSJ. Microstructural changes in alkali activated fly ash/slag geopolymers with sulfate exposure. Mater Struct 2013;46(3):361–73.
[44] Deira E, Gebregziabiher BS, Peethamparan S. Influence of starting material on the early age hydration kinetics, microstructure and composition of binding gel in alkali activated binder systems. Cem Concr Compos 2014;48:108–17.
[45] Chithiraputhiran S, Neithalath N. Isothermal reaction kinetics and temperature dependence of alkali activation of slag, fly ash and their blends. Constr Build Mater 2013;45:233–42.
[46] Brough AR, Holloway M, Sykes J, Atkinson A. Sodium silicate-based alkali-activated slag mortars Part II. The retarding effect of additions of sodium chloride or malic acid. Cem Concr Res 2000;30:1375–9.
[47] Ravikumar D, Neithalath N. Reaction kinetics in sodium silicate powder and liquid activated slag binders evaluated using isothermal calorimetry. Therm acta 2012;546:32–43.
[48] Shi C, Day RL. A calorimetric study of early hydration of alkali-slag cements. Cem Concr Res 1995;25:1333–46.
[49] Lothenbach B, Saout GL, Gallucci E, Scrivener K. Influence of limestone on the hydration of Portland cements. Cem Concr Res 2008;38:848–60.
[50] Pera J, Husson S, Guilhot B. Influence of finely ground limestone on cement hydration. Cem Concr Compos 1999;21(2):99–105.
[51] Rajaokarivony AZ, Thomassin JH, Baillif P, Touray JC. Experimental hydration of two synthetic glassy blast furnace slags in water and alkaline solutions (NaOH and KOH 0.1 N) at 40 °C: structure, composition and origin of the hydrated layer. J Mater Sci 1990;25(5):2399–410.
[52] Zhang ZH, Wang H, Provis JL, Bullen F, Reid A, Zhu YC. Quantitative kinetic and structural analysis of geopolymers. Part 1. The activation of metakaolin with sodium hydroxide. Therm Acta 2012;539:23–33.
[53] Hajimohammadi A, Provis JL, Deventer JSJ. Time-resolved and spatially resolved infrared spectroscopic observation of seeded nucleation controlling geopolymer gel formation. J Colloid Interface Sci 2011;357:384–92.
[54] Criado M, Fernandez-Jimenez A, Palomo A. Alkali activation of fly ash: Effect of the SiO_2/Na_2O ratio Part I: FTIR study. Microporous Mesoporous Mater 2007;106:180–91.
[55] Yu P, Kirkpatrick RJ, Poe B, McMillan PF, Cong X. Structure of calcium silicate hydrate (C–S–H): near-, mid-, and far-infrared spectroscopy. J Am Ceram Soc 1999;82(3):742–8.
[56] Thongsanitgarn P, Wongkeo W, Chaipanich A, Poon CS. Heat of hydration of Portland high-calcium fly ash cement incorporating limestone powder: effect of limestone particle size. Constr Build Mater 2014;66:410–7.
[57] Voglis N, Kakali G, Chaniotakis E, Tsivilis S. Portland-limestone cements. Their properties and hydration compared to those of other composite cements. Cem Concr Compos 2005;7:191–6.
[58] Kakali G, Tsivilis S, Aggeli E, Bati M. Hydration products of C_3A, C_3S and Portland cement in the presence of $CaCO_3$. Cem Concr Res 2000;30:1073–7.
[59] De Weerdt K, Ben Haha M, Le Saout G, Kjellsen KO, Justnes H, Lothenbach B. Hydration mechanisms of ternary Portland cements containing limestone powder and fly ash. Cem Concr Res 2011;41:279–91.
[60] Kong DLY, Sanjayan JG. Effect of elevated temperatures on geopolymer paste, mortar and concrete. Cem Concr Res 2010;40:334–9.
[61] Alarcon-Ruiz L, Platret G, Massieu E, Ehrlacher A. The use of thermal analysis in assessing the effect of temperature on a cement paste. Cem Concr Res 2005;35:609–13.
[62] Rovnaník P, Bayer P, Rovnaníková P. Characterization of alkali activated slag paste after exposure to high temperatures. Constr Build Mater 2013;47:1479–87.
[63] Escalante García JI, Campos-Venegas K, Gorokhovsky A, Fernández A. Cementitious composites of pulverised fuel ash and blast furnace slag activated by sodium silicate: effect of Na_2O concentration and modulus. Adv Appl Ceram 2006;105(4):201–8.
[64] Shen WG, Wang YH, Zhang T, Zhou MK, Li JS, Cui XY. Magnesia modification of alkali-activated slag fly ash cement. J Wuhan Univ Technol-Mater. Sci. Ed. 2011;26:121–5.
[65] Tsivilis S, Chaniotakisb E, Badogiannis E, Pahoulasa G, Ilias A. A study on the parameters affecting the properties of Portland limestone cements. Cem Concr Compos 1999;21:107–16.
[66] De Weerdt K, Kjellsen KO, Sellevold E, Justnes H. Synergy between fly ash and limestone powder in ternary cements. Cem Concr Compos 2011;33:30–8.
[67] Wang SD, Scrivener KL. ^{29}Si and ^{27}Al NMR study of alkali-activated slag. Cem Concr Res 2003;33:769–74.
[68] Richardson IG. Tobermorite/jennite- and tobermorite/calcium hydroxide-based models for the structure of C–S–H: applicability to hardened pastes of tricalcium silicate, β-dicalcium silicate, Portland cement, and blends of Portland cement with blast-furnace slag, metakaolin, or silica fume. Cem Concr Res 2004;34:1733–77.
[69] Fernández-Jiménez A, Puertas F. Structure of calcium silicate hydrates formed in alkaline-activated slag: influence of the type of alkaline activator. J Am Ceram Soc 2003;86(8):1389–94.
[70] Zajac M, Rossberg A, Le Saoût G, Lothenbach B. Influence of limestone and anhydrite on the hydration of Portland cements. Cem Concr Compos 2014;46:99–108.
[71] Chen W. Hydration of slag cement: theory, modeling and application, Ph.D. Thesis, Eindhoven University of Technology, The Netherlands; 2007. p. 1–223.